Dimensioning radial prosumer-based thermal networks

Fabian SPEER (1), Thomas LICKLEDERER (1), Daniel ZINSMEISTER (1), Vedran S. PERIĆ (1)

(1)Technical University of Munich (TUM)
Munich Institute of Integrated Materials, Energy and Process Engineering (MEP),
Lichtenbergstraße 4a, 85748 Garching b. München, fabian.speer@tum.de

Abstract:

The energy flows in prosumer-based based thermal networks are volatile, thus the problem of dimensioning the network infrastructure is more challenging than in the case of conventional unidirectional thermal networks. This paper introduces a rule-based method to determine the relevant design parameters of network pipes, control valves, and circulation pumps in radial prosumer-based networks. The dimensioning is performed based on the calculated maximal power flows through each pipe section of the network. The required inputs for the method are secondary side prosumer characteristics. The method is implemented in Excel and its application is demonstrated on a case study with a network with five residential prosumers. The method's accuracy and the functionality of dimensioned components were benchmarked under different energy exchange scenarios with a detailed thermohydraulic grid model implemented in Modelica using *Dymola*. The validation criteria were (i) the accuracy of the calculated maximal power flows in the network pipes, (ii) supply of consumers with the designed power and supply temperature (iii) the actuator operating points. Criterium (i) was achieved with a maximal error of *0.7 %*. Criterium (ii) was met in all exchange scenarios with maximal deviations of *3.3 %* for delivered power and *0.58 K* for supply temperature. In criterium (iii), control errors in the primary temperature spread lead to deviations in the operating points. However, they remained in an operable range and did not impair the network's functionality. Thus, the introduced method allows to dimension flexible prosumer-based networks with limited information during early-stage economic analyses and variant comparisons.

Keywords: district heating, prosumer-based network, dimensioning method, planning tool, network components

1 Introduction

1.1 Motivation

Conventional thermal networks (*CNs*) use a central generation unit to provide thermal energy. Central circulation pump(s) in a network of supply and return pipes drive a unidirectional mass flow to distribute the energy to consumers. Due to the unidirectional flows in *CN*s, each network section (pipe, substation) is part of a fixed hydraulic circuit (see Figure 1, A and B). Various tools and guides exist to dimension *CN*s with state of the art methods [1–6]. In those guides, the worst conditions for each network section in its hydraulic circuit build the design state for dimensioning.

Including prosumers in *CN*s can be advantageous for energy efficiency and network flexibility [7, 8]. This paper considers the most extreme form of prosumer integration: a prosumer-based thermal network (*PBN*) comprised only of prosumers without any dominating central unit. Decentral actuators (pumps and control valves) in the substations enable bidirectional mass and energy flow in the network for load-balancing between prosumers [9]

In *PBN*s, in contrast to *CN*s, each specific network section is part of varying hydraulic circuits. This phenomenon is caused by bidirectional flows in the network and influenced by changing prosumer modes and load scenarios (see Figure 1, C and D). Thus, the question arises of how to dimension such networks.

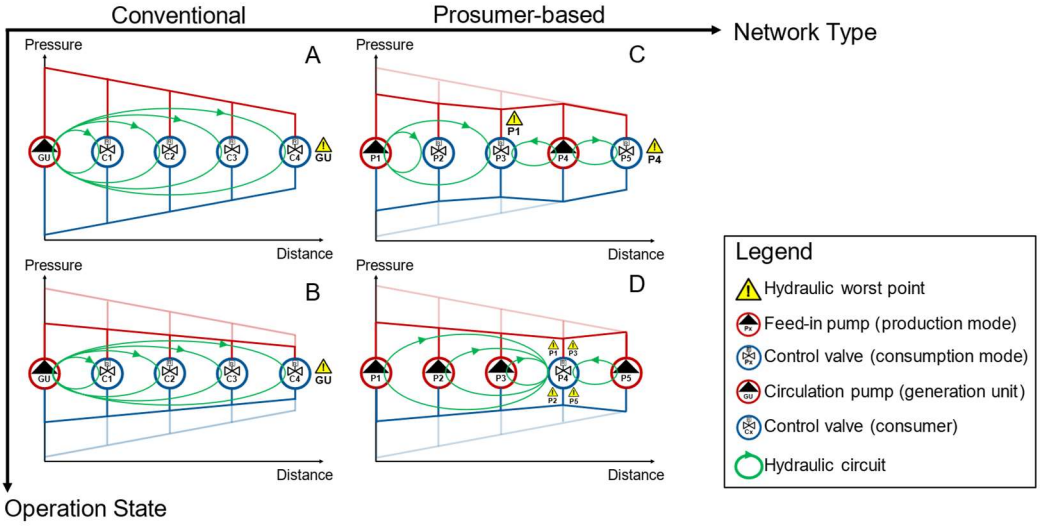

Figure 1: Comparison of pressure curves and hydraulic circuits in different operation states of a thermal network (A and B) with central generation unit vs. prosumer-based network (C and D).

Various models and simulations have been built to optimize the operation and design of components in thermal networks with bidirectional mass flow [10–12]. However, to the best of the authors knowledge, there is no tool for dimensioning such networks, while the number of planners with experience in pilot projects is very limited [7, 13]. Thus, comparisons between *CN* and *PBN* for variant decisions in early project stages require simulations and are prone to inconsistency [7, 14]

The basis for thermal dimensioning procedures is the design power flow. Due to the hydraulic flexibility of *PBN*s described earlier, the design power in the network components depends on other prosumers. Thus, determining the significant power flows is the necessary preliminary stage for component design in radial *PBN*s.

In this paper we propose a method to identify the hydraulic circuit, power flows and prosumer load situations relevant to the design of primary side network components in radial *PBN*s. It is structured as follows: First the considered network structure is characterized. An algorithm to determine the relevant power flows for dimensioning in this network structure is proposed. An Excel tool for dimensioning the core network components, i.e. feed-in pumps (*FIP*s), control valves (*CoV*s), and network pipes is introduced. In a case study a network with 5 prosumers is dimensioned with the tool and a simulation with different exchange scenarios is used to validate the functionality of the dimensioned components.

1.2 Network concept

The structure and the main components of the considered *PBN* are depicted in Figure 2. The *FIP* and *CoV* are the decentral actuators, which influence the pressure and mass flow on the primary network side, while the production pump (*ProP)* and the consumption pump (*ConP)* control the mass flow on the secondary side. When the prosumer is in production mode, *FIP* and *ProP* are active; *CoV* is closed, and *ConP* is inactive. In consumption mode, FIP and ProP are inactive, while CoV is open and ConP is active. In this paper, to prove the concept of the method, only a radial network configuration with a main distribution line and direct connection lines is considered.

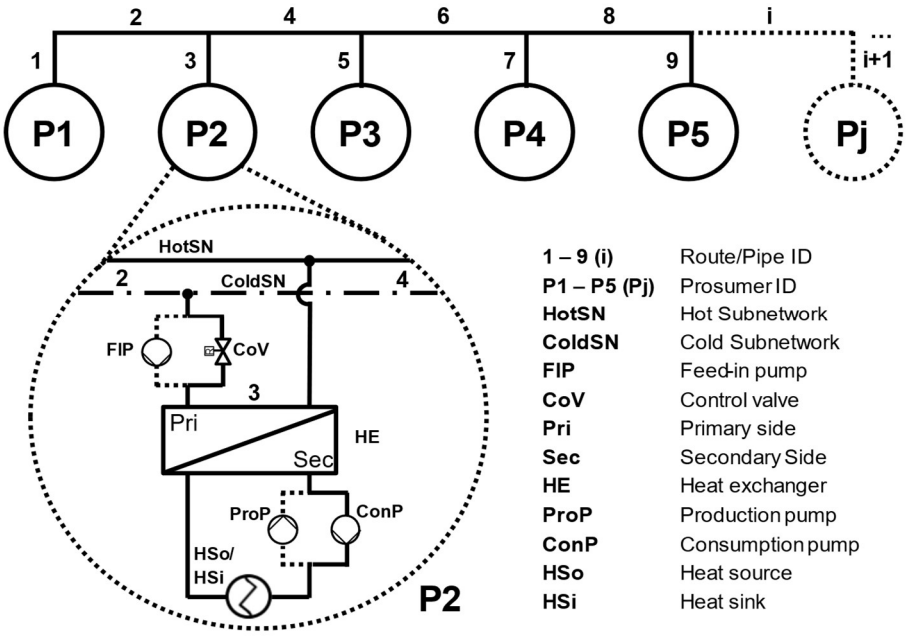

Figure 2: Structure of a radial prosumer-based network

2 Dimensioning Method

The dimensioning method was developed for two flexibility design premises to give upper and lower boundaries for component dimensioning depending on the targeted operation flexibility:

- All-Neighbor-Exchange (*ANE*): Each prosumer can exchange energy with each of the other prosumers in the network.
- One-Neighbor-Exchange (*ONE*): Each prosumer can only exchange energy with directly neighboring prosumers.

Throughout this paper the design premise *ANE* is assumed.
Table 1 lists the necessary input parameters and the values used for the case study.

Table 1: User input parameters and values applied in the case study

Description	Symbol	Value	Unit
Medium in the network pipes	Medium	Water	–
Type of network pipes	Piping type	Plastic jacket pipes	–
Length of the route sections	l_{route}	see Table 6	m
Maximum flow velocity in connection pipes	$u_{max}^{pipe,cct}$	1	m/s
Maximum flow velocity in distribution pipes	$u_{max}^{pipe,dis}$	1.5	m/s
Maximum pressure gradient in connection pipes	$R_{max}^{pipe,cct}$	250	Pa/m
Maximum pressure gradient in distribution pipes	$R_{max}^{pipe,dis}$	250	Pa/m
Target temperature in the hot subnetwork	$\vartheta_{hot,tar}^{prim}$	65	$°C$
Target temperature in the cold subnetwork	$\vartheta_{cold,tar}^{prim}$	50	$°C$
Targeted valve authority	a_{tar}^{CoV}	0.5	–
Assumed pressure gradient in individual resistors (e.g. fittings)	R_{ir}	10	%
Maximal prosumer consumption power	$P_{max}^{pros,con}$	see Table 3	kW
Maximal prosumer production power	$P_{max}^{pros,pro}$	see Table 3	kW
Target secondary supply temperature consumption mode	$\vartheta_{hot,tar}^{sec,con}$	60	$°C$
Set secondary return temperature in consumption mode	$\vartheta_{cold,set}^{sec,con}$	45	$°C$
Pressure loss through heat exchangers in design conditions	Δp_{HE}^{prim}	20	kPa
Design temperature difference in the heat exchangers	ΔT_{HE}	3	K

Symbols		Sub- and superscripts		Abbreviations	
l	Length	cct	Connection	PBN	Prosumer-based network
u	Velocity	dis	Distribution	CN	Conventional network
R	Pressure gradient	con	Consumption	FIP	Feed-in pump
Δp	Pressure loss	pro	Production	CoV	Control valve
H	Pump head	tar	Target	DHC	Design hydraulic circuit
ϑ	Temperature °C	$prim$	Primary side	Sc	Exchange scenario
T	Temperature K	sec	Secondary side	ANE	All-Neighbor-Exchange
a	Valve authority	$pros$	Prosumer	ONE	One-Neighbor-Exchange
P	Prosumer power	HE	Heat exchanger	P1	Prosumer with ID 1
$\dot{Q}$	Transported power	ir	Individual resistors	DHW	Domestic hot water
D	Diameter	$pipe$	Network pipe		
K	Flow coefficient	max	Maximal		
		set	Set point		

2.1 Determining the design power flows - algorithm

In Figure 3, an example application of the proposed algorithm to determine the maximal power flows $\dot{Q}^{i}_{max}$ in the network pipes as design conditions is depicted. The algorithm is built for radial *PBN* with a network structure and nomenclature as shown in Figure 2.

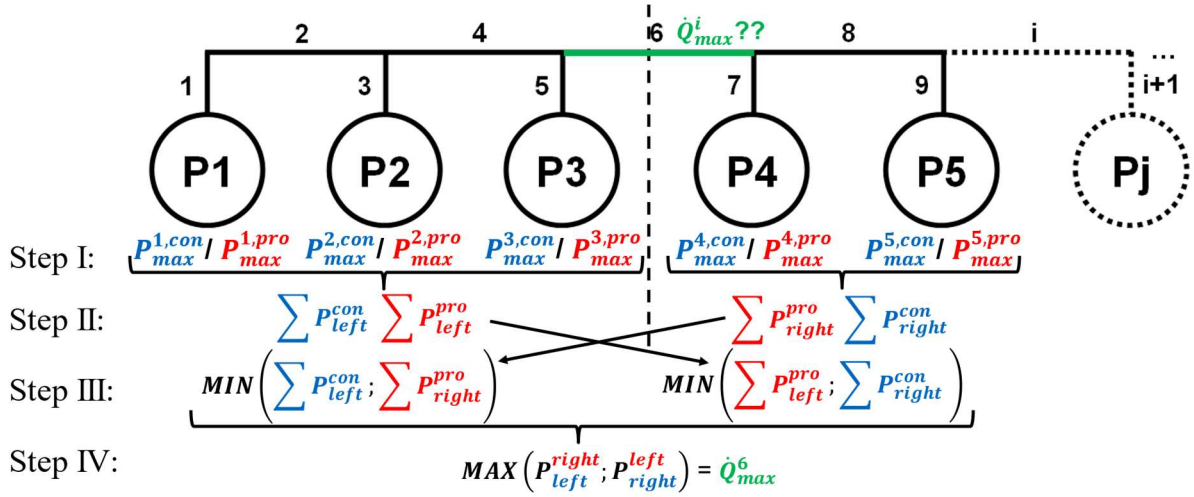

Figure 3: Algorithm for determining the design power flows in an example distribution pipe

The algorithm describes four main steps to determine the maximum power flow through the network pipes of a radial *PBN*. In *Step I* the network is split into two sides, relative to the considered pipe (i.e. pipe 6). The maximal consumption power $P^{j,con}_{max}$ and the maximal production power $P^{j,pro}_{max}$ are set for each prosumer. In *Step II* the available demand and supply power of both network sides are calculated by adding up the consumption and production power of the prosumers. With this, the relevant demand and supply from the left and the right side of the network are determined. The power flow in the pipe is characterized by the energy exchange from one side to another. Thus, in *Step III* the possible power exchanges between the two sides is determined. This is done by comparing the maximum supply power of one side to the maximum demand power from the other side. The smaller value between those describes the possible power exchange. Finally, in *Step IV* the maximum of the two possible power exchanges is calculated to result in the design power flow $\dot{Q}^{6}_{max}$ of pipe 6. A more detailed flow chart for determining the power flow in all network pipes is included in the appendix (see Figure 10).

2.2 Component dimensioning

The remaining dimensioning procedure follows established methods described in Ref. [3]. The flow chart describing the main dimensioning steps and target values is depicted in Figure 4.

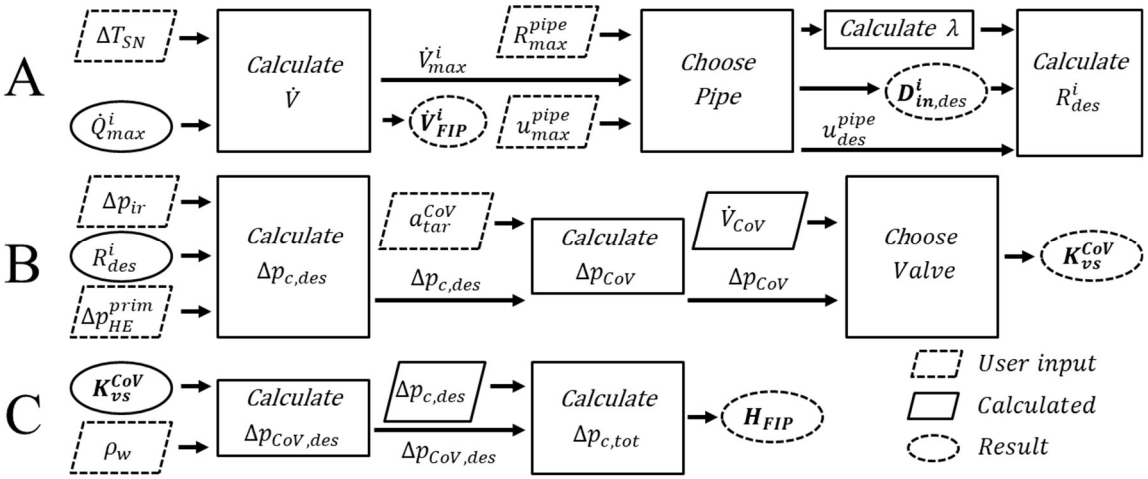

Figure 4: Flow chart for the component dimensioning

2.2.1 Pipe Dimensioning

The procedure for pipe dimensioning is depicted in **A** (see Figure 4). The pipes are dimensioned, based on the maximum transported power $\dot{Q}^i_{max}$ determined in subsection 2.1. The user-defined values for the maximum conditions in connection and distribution pipes (see Table 1) are considered.

The friction factor λ is calculated using the approximation of the Colebrook's equation described in [15].

2.2.2 Control valve Dimensioning

The procedure for *CoV* dimensioning is depicted in **B** (see Figure 4). The hydraulic circuit with the maximum pressure loss $\Delta p_{c,des}$ between a consuming and a producing substation (*CoV* excluded) is the design hydraulic circuit (*DHC*) for the *CoV*. The theoretical *CoV* pressure drop is calculated with $\Delta p_{c,des}$ and a^{CoV}_{tar} set in Table 1 (eq. (1)). To limit the pressure losses, the next larger available *CoV* is chosen.

$$a^{CoV}_{tar} = \frac{\Delta p_{CoV,th}}{\Delta p_{CoV,th} + \Delta p_{c,des}} \quad (1)$$

2.2.3 Pump Dimensioning

The $\Delta p_{CoV,des}$ is calculated with K^{CoV}_{vs} determined in **B** [3]. The head for the *FIP* H^{FIP}_{des} (see **C** Figure 4) is then specified by the resulting total pressure drop in the *DHC* $\Delta p_{c,tot}$. The volume flow $\dot{V}^{FIP}_{des}$ is determined in **A** (see Figure 4) along with the volume flows in the network pipes.

3 Dimensioning Tool

An Excel tool was built to automate the dimensioning process. The parameters, algorithm and dimensioning procedure from section 2, alongside the nomenclature from Figure 2 are implemented in the tool.

It is published at: https://github.com/FabianSpeer/PBN_Dimensioning_Tool. It provides the structure to dimension a *PBN* with a maximum of 20 prosumers (with limits to the available product sizes).

Example products are used for dimensioning, as shown in Table 2. The relevant values from the manufacturer data sheets of the product lines are included in the tool.

Table 2: Product lines and manufacturers of primary network components used in the case study

Component	Manufacturer	Product line
Pipes	ISOPlus [16]	Plastic jacket pipes (standard)
Control valves	Sauter [17]	VUN
Circulation pumps	Grundfos [18]	CR – inline pumps

For each component, the calculated dimensioning results are considered the minimum requirements.

4 Case study

The dimensioning method is validated by implementing its results in a thermohydraulic simulation and comparing the results.

The validation criteria are:

i. Accuracy of the predicted design power flows in network pipes $(\dot{Q}^{i}_{max})$
ii. Sufficient consumer supply with power demand $(\dot{Q}^{j}_{con})$ and supply temperature (ϑ^{sec}_{hot})
iii. Actuator states: valve opening (κ^{CoV}_{set}), pump speed (u^{FIP}_{set}) and operating state $\Delta p(\dot{V})$

4.1 Setup

The introduced dimensioning tool is used to dimension the network components, as described in sections 2 and 3. The dimensioned components are implemented into a thermohydraulic grid model. The *ProsNet* [20] library was used to build the model in the Modelica-based software *Dymola* [19]. During the simulation, the actuators are controlled by a specially modeled weighted PID controller [20] to achieve the temperatures and power flows specified in Table 1.

4.1.1 Prosumer side

The prosumers are based on the five residential houses emulated in the *CoSES*-laboratory [21]. Due to the proposed early-stage application of the dimensioning method, the houses are categorized into TABULA building typologies [22] to determine their heat demands. Their properties and resulting demands are listed in Table 3.

Ventilation and transmission losses of the houses were calculated according to the simplified procedure of the *DIN EN 12831-1* for the climate in Munich, using the respective heat transfer coefficients stated in the TABULA typologies.

For the power demand for domestic hot water (DHW), the peak flows were determined according to the *DIN 1988-300*. The required additional power was calculated for temperatures described in *DIN 12831-3 A100*. A DHW storage with a discharge time of 10 min (*DIN 4708-1*) and a recharge time of 60 min was assumed.

All prosumers are assumed to be equipped with heat sources capable of generating 100 % of their total heat demand, as suggested in [23].

Table 3: Prosumer characteristics in the case study

	P1	***P2***	***P3***	***P4***	***P5***
Living Area [m²]	300	400	300	750	300
No. of Apartments	1	3	2	4	2
Age Class	1995 - 2002	From 2016	2007 – 2009	1995 – 2002	2007 - 2009
TABULA Code	SFH.09.Gen	SFH.12.Gen	SFH.10.Gen	MFH.09.Gen	SFH.10.Gen
TABULA Standard	Improved	Improved	Improved	Improved	Improved
Heat loss transmission [kW]	13.0	9.9	8.9	16.7	8.9
Heat loss ventilation [kW]	5.2	1.1	4.3	13.0	4.3
Heat demand DHW [kW]	7.1	10.5	8.1	12.2	8.1
Total heat demand [kW]	25.3	21.5	21.2	41.8	21.2

4.1.2 Network side

The parameters of primary side components are chosen according to the results from the dimensioning tool with the conditions described in Table 1 and Table 2. The selected component sizes are documented in the appendix (see Table 6-Table 8).

4.1.3 Scenarios

The exchange scenarios (*Sc*) were chosen to create a consumption design state and production design state for each prosumer at least once. Two criteria must be fulfilled for a prosumer to be in its design state. First, it must operate with its maximum production or consumption power (see Table 3). Second, the transported power flow in their design hydraulic circuit (DHC) (see Figure 5) is maximal, as defined by the algorithm in subsection 2.1.

In Figure 5 the qualitative pressure curves and set prosumer powers in two example scenarios are shown. In scenario 1 the production design states for the *FIP*s 1 and 2, and the consumption design state for the *CoV*s 4 and 5 are observed. Prosumer 3 is operating in part-load, since the prosumer powers set in Table 3 do not allow all prosumers to be in a design state simultaneously. Consequently a separate scenario is required to achieve the design states described above for prosumer 3. The chosen design scenario for the *FIP3* is also shown in Figure 5, where prosumers 1,2 and 3 operate under maximum loads, while prosumers 4 and 5 operate in part-load.

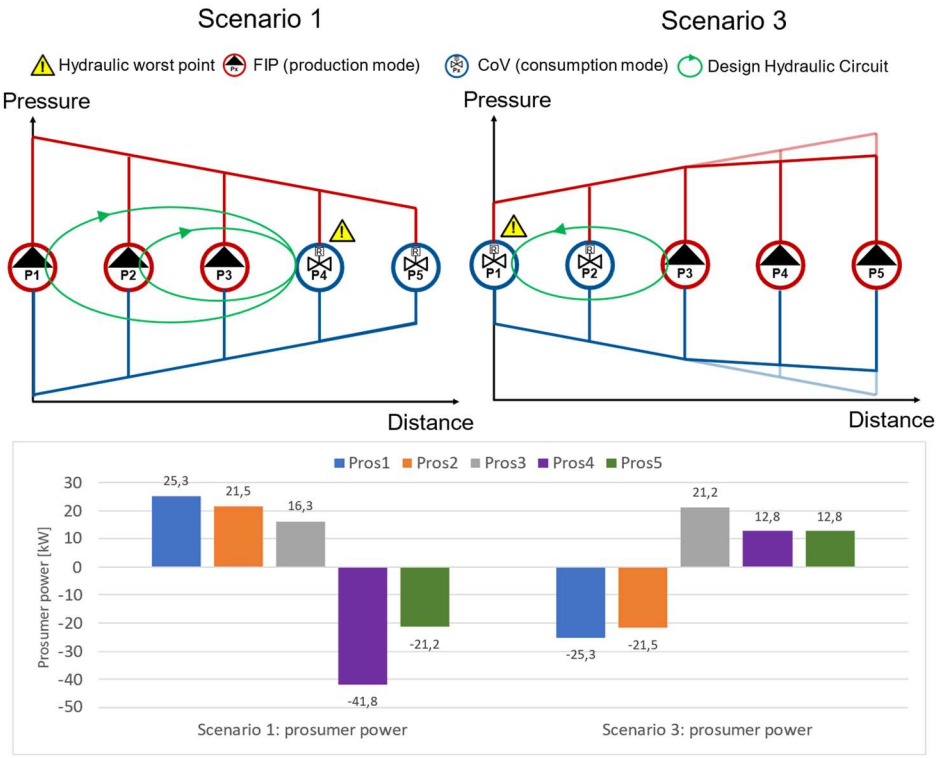

Figure 5: Qualitative pressure curves and prosumer power in example exchange scenarios 1 and 3 with design conditions for FIP1&2 and CoV4&5 in scenario 1 and for FIP3 in scenario 3

Since the consumption power is as high as the production power for all prosumers, the missing design states can be achieved by inverting the power flow of all prosumers during scenarios 1 and 3. By doing so the production design scenario for the *FIP* of a prosumer turns into the consumption design scenario for the *CoV* of the prosumer.

The inverted *Sc1* is named *Sc2* and the inverted *Sc3* describes *Sc4*. The relevant design scenarios for all actuators are listed in Table 4.

Table 4: Design scenarios for the actuators

	Scenario 1		Scenario 2		Scenario 3		Scenario 4	
Design scenario for:	FIP	1 & 2	FIP	4 & 5	FIP	3	FIP	-
	CoV	4 & 5	CoV	1 & 2	CoV	-	CoV	3

Additionally, the observation of the network behavior in part-load situations is desired. Thus, 2 additional scenarios (5 and 6) are created, which correspond to half the power flows of scenario 1 and 2 respectively.

The secondary supply temperature $\vartheta^{sec}_{hot,pro} = \vartheta^{prim}_{hot,tar} + \Delta T_{HE}$ is set according to the inputs from Table 1 to *68 °C* during production, and the return temperature $\vartheta^{sec}_{cold,con}$ is set to *45 °C* during consumption for every prosumer to exclude the performance of the secondary heat source/sink from the analysis.

Each scenario is simulated for 1 hour with simulation steps of 10 seconds. Before and after each scenario, transition states with half the power are set for 15 minutes.

4.2 Simulation results

For evaluating the proposed dimensioning method, only the steady-state operation is relevant. Thus, the following values are read at the end of each 1-hour simulation section when the operation state has stabilized.

The design values for the error analyses of pipes and actuators are documented in the appendix (see Table 6 - Table 8). The design values for prosumers can be extracted from Table 3.

The absolute errors ($\boldsymbol{\varepsilon}$) for the maximum simulated power flows $\dot{Q}^{i}_{max,sim}$ and the maximum volume flow $\dot{V}^{i}_{max,sim}$ in the 9 pipe sections are shown in Figure 6.

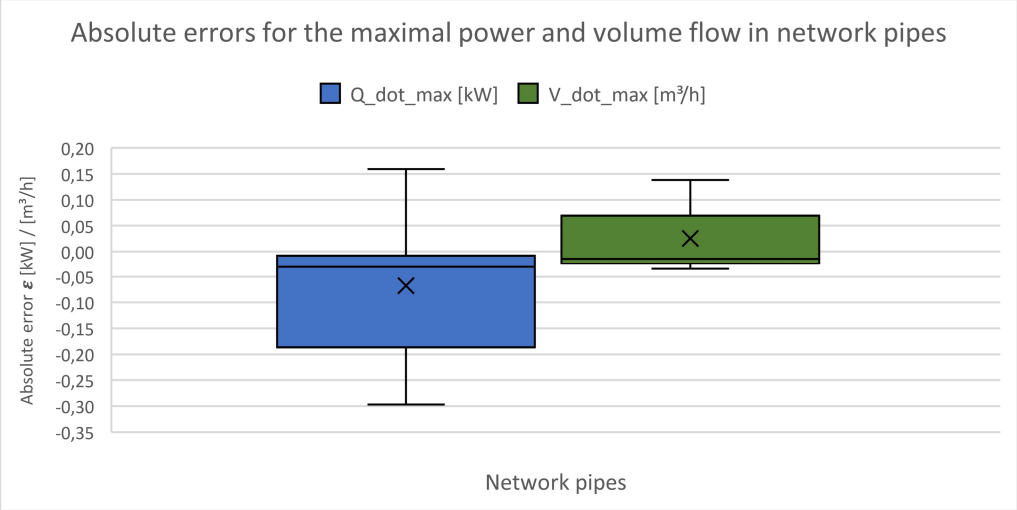

Figure 6: Absolute errors for simulated $\dot{Q}^{i}_{max,sim}$ and $\dot{V}^{i}_{max,sim}$ compared to design $\dot{Q}^{i}_{max}$ and $\dot{V}^{i}_{max}$ in the network pipes

The maximal relative deviation for $\dot{Q}^{i}_{max}$ is *0.7 %* and occurs during Sc3. The small errors for $\dot{Q}^{i}_{max}$ indicate, that the algorithm presented in 2.1 can accurately predict the design power flows in the network pipes. Thus, the first (i) validation criterium is fulfilled. The maximal relative deviation for $\dot{V}^{i}_{max}$ is *5.5 %* in pipe sections 8 and 9 during Sc1. This increases the pressure gradient in the pipe compared to the design value. However, with the chosen pipe dimensions (see Table 6) the pressure gradient is still below the set maximum of *250 pa/m*.

Figure 7 depicts the absolute errors for $\dot{Q}_{con}^{j}$ and ϑ_{hot}^{sec} that resulted from the simulation of the prosumers during their design (*des*) scenario and during part load (*pl*) scenarios *Sc5* and *Sc6* as defined in subsection 4.1.3.

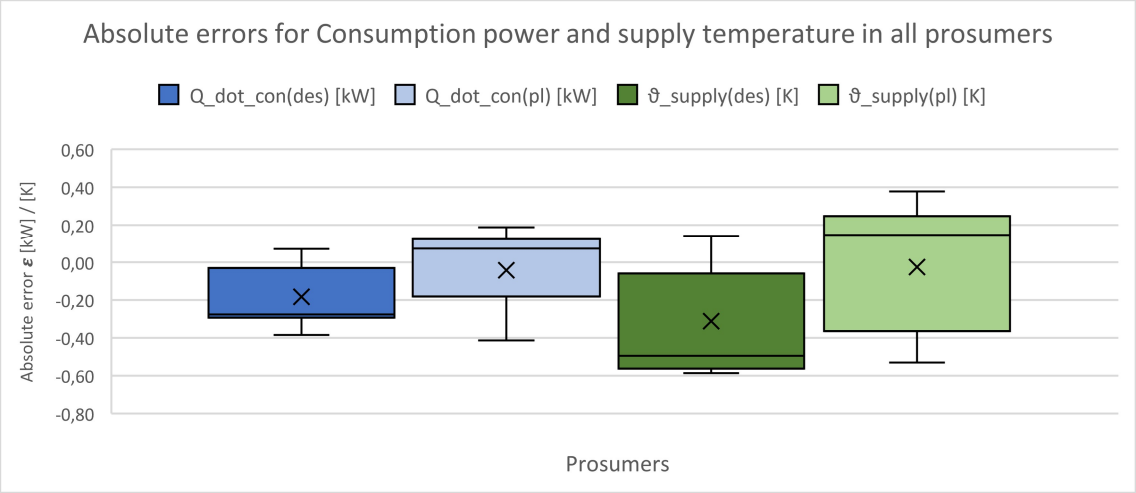

Figure 7: Simulated and design values for $\dot{Q}_{con}^{j}$ and ϑ_{hot}^{sec} during design and part load consumption scenarios

The maximal relative error for $\dot{Q}_{con}^{j}$ is *1.5 %* during design conditions in Sc2 and *3.3 %* in the part-load scenario 6. The maximal relative deviation of ϑ_{hot}^{sec} is *-0.58 K* during design conditions in Sc4 and *-0.53 K* in the part-load scenario 6. The recorded errors have no significant not impact on the operation of the connected prosumers with a setpoint supply temperature of $\vartheta_{hot}^{sec} = 60\,°C$. Consequently, the consumption demands of all prosumers are met during every scenario. Thus, the second (ii) validation criterium can also be regarded as fulfilled.

In the third (iii) criterium, the actuator operating states are considered. The operating states are defined by volume flow $\dot{V}$ through and the pressure difference Δp over the actuator. Since the differential pressure and the volume flow depend on each other, a volume flow error also causes deviations from the designed differential pressure of the actuator. Volume flow errors were already recorded in the network pipes (see Figure 6). These deviations must result from an error in the temperature spread $\Delta T_{set}^{prim} = \vartheta_{hot,set}^{prim} - \vartheta_{cold,set}^{prim}$, since the power flows in the pipes matched the design nearly perfectly and the two values are connected by eq. (2).

$$\dot{Q}_{des}^{pipe} = c * \dot{V} * \Delta T_{set}^{prim} \tag{2}$$

Where c is a combined constant of the density and heat capacity of the medium.

With the described impact on the volume flow, the errors for ΔT_{set}^{prim} shown in Figure 8, have direct impact on the operating point deviations of the actuators.

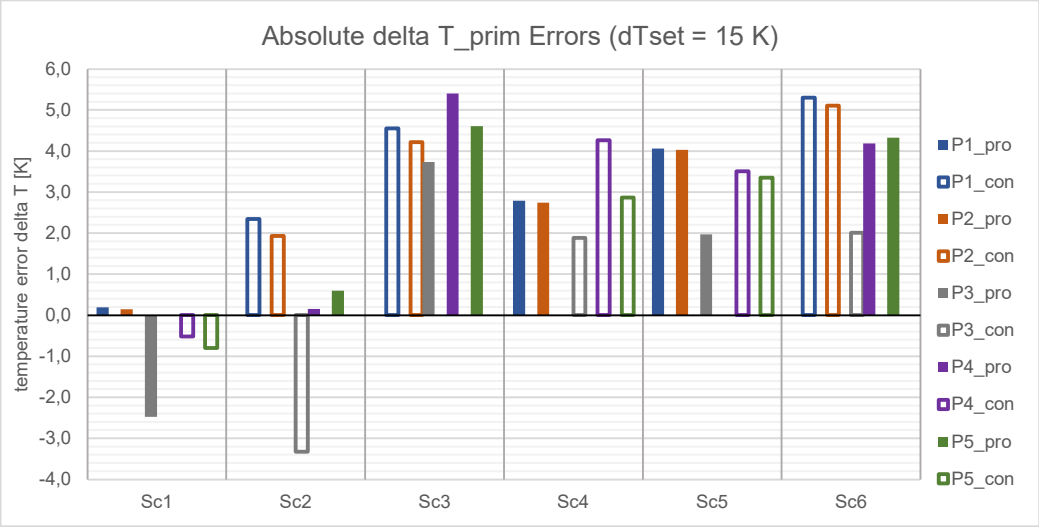

Figure 8: Absolute error $\varepsilon(\Delta T_{set}^{prim})$ across all scenarios

It is noticeable, that the errors in Figure 8 are mostly positive and thus cause a reduced volume flow. The errors are at their lowest, during the scenarios 1 and 2, when the energy exchange in the network is the highest. The control objectives of the used weighted PID controller [20] are still undergoing research. Thus, control errors are likely to be the cause of the deviations.

Table 6 shows the normalized control values for the *FIP* speed, and the *CoV* opening in a range from *0* to *1* during their respective design scenarios.

Table 5: Normalized speed of FIPs u_{set}^{FIP} and opening of CoVs κ_{set}^{CoV} at their operating points

Normalized values	P1	P2	P3	P4	P5
u_{set}^{FIP} [0..1]	0.80	0.74	0.56	0.80	0.70
κ_{set}^{CoV} [0..1]	1.00	0.80	1.00	1.00	0.93

The maximum u_{set}^{FIP} value of *0.8* in Table 5 shows that the designed pumps allow for expansion of the *PBN* at hand. The κ_{set}^{CoV} is *1* for the prosumers at the critical point during their consumption design scenario (see Figure 5), as intended to minimize pressure losses. For *P2* and *P5* $\kappa_{set}^{CoV} < 1$ to adjust to the pressure conditions created by the remaining prosumers in *Sc1* and *Sc2* (see Figure 5). Thus, the actuator control in general works as intended, but the errors in Figure 8 suggest the built in prioritization of the controller causes deviations from the set conditions during part-load situations.

In Figure 9, the dimensioned operating point of each actuator is compared to the operating point resulting from the simulation of their design scenario (see Table 4). Additionally, the pump curves of the two *FIP* types (see Table 8) at maximum speed ($\boldsymbol{u_{max}^{FIP}}$) are displayed.

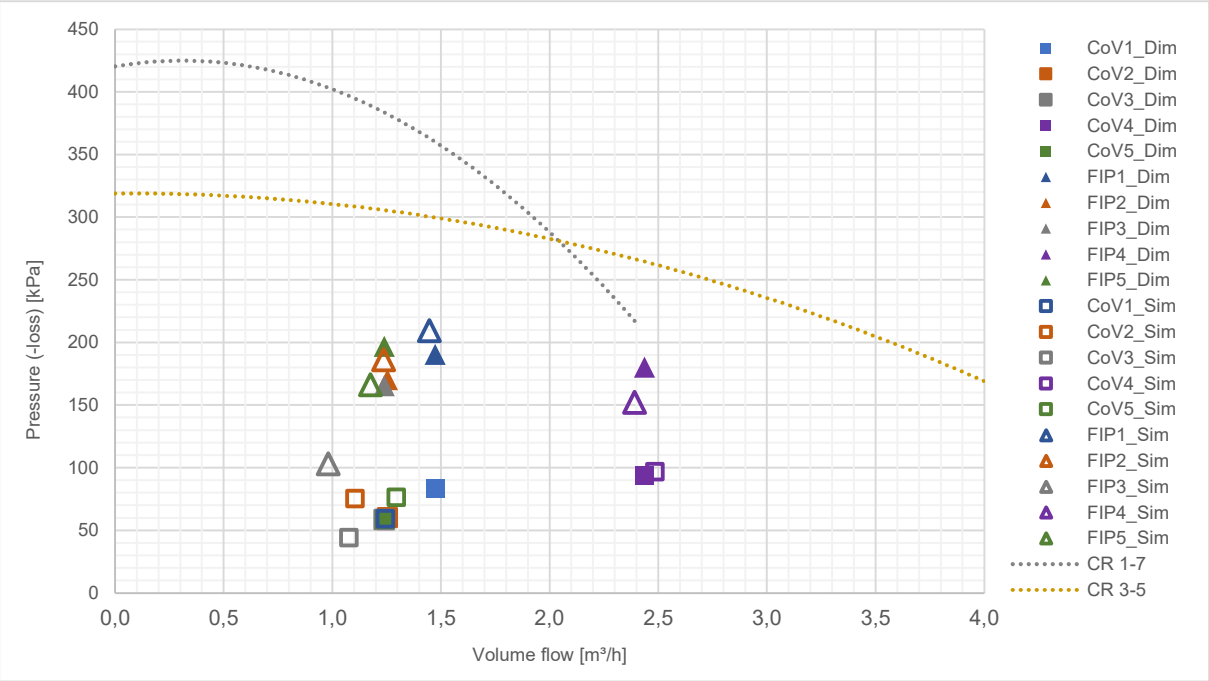

Figure 9: Pump curves ($\boldsymbol{u_{max}^{FIP}}$) and dimensioned and simulated operation states of FIPs and CoVs during design states

The operating point deviations of the actuators (*FIP3*, *CoV3*, *FIP5*, *FIP4* and *CoV1*) can be explained by the positive $\boldsymbol{T_{set}^{prim}}$errors at the consuming *P1* in *Sc1* and Sc*3* and the consuming *P4* in *Sc4*. It is notable that *FIP1,* despite a positive $\boldsymbol{T_{set}^{prim}}$error during *Sc1* features a higher pressure increase than expected. That is because in *Sc1* the $\boldsymbol{T_{set}^{prim}}$error at the *CoV4* in the *DHC* of *FIP1* is negative due to the large negative $\boldsymbol{T_{set}^{prim}}$error at the part load *FIP3*. The difference between the simulation and design for *CoV2* and *CoV5* stems from a combination of $\boldsymbol{T_{set}^{prim}}$errors and the partially closed state of the *CoV*s $\boldsymbol{\kappa_{set}^{CoV2} = 0.8}$ during *Sc2* and $\boldsymbol{\kappa_{set}^{CoV5} = 0.93}$ in *Sc1* (see Table 5).

Due to the $\boldsymbol{T_{set}^{prim}}$errors, the predicted network states are not recreated fully in the simulation. However, since the deviations at the design load scenarios *Sc1* and *Sc2* are relatively small, the case study still yields relevant results for the validating the dimensioning method under the third (iii) criterium. Furthermore, the positive outcomes in the second (ii) validation criterium showed, that the different operating points did not impair the network's functionality.

A pump blocking effect, described in previous work [24] on *PBN*s could not be observed in the simulated exchange scenarios. Pump blocking is likely mitigated by the used design method for the pump, which considers the pressure conditions created by other prosumers at the feed-in location.

5 Conclusion and outlook

The simulation results showed that the dimensioning tool is well suited to dimension *PBN* components with limited information. Thus, the proposed method can be used in early-stage dimensioning, to dimension components capable of a functional network operation during different load scenarios.

The proposed method in its current state has a few limitations: It is restricted to a radial heat network. More complex networks with interconnections are not implemented yet. Additionally, the demand and temperatures of the secondary heat sources and sinks were assumed as static inputs. Furthermore, the provided tool is currently limited to two exchange premises.

Additional research regarding *PBN* dimensioning should aim to advance the dimensioning method towards more complex network typologies and conduct tests for different distributions of source and sink powers at the prosumers. The combination of the *PBN* structure with principles of 5th generation district heating and cooling networks could provide additional benefits for flexibility and efficient energy exchange. The coupling with secondary load and production models for a dynamic simulation with included environmental influences on the prosumer side should be targeted to represent the networks' robustness precisely.

The provided dimensioning tool in its current state offers a quick way to dimension the core network components of small-scale radial *PBN*s. Thus, our developed method allows to include this innovative network type for neighborhood solutions in early-stage variant comparisons and provides realistic component sizes for planners to use in economic analyses.

6 Appendix

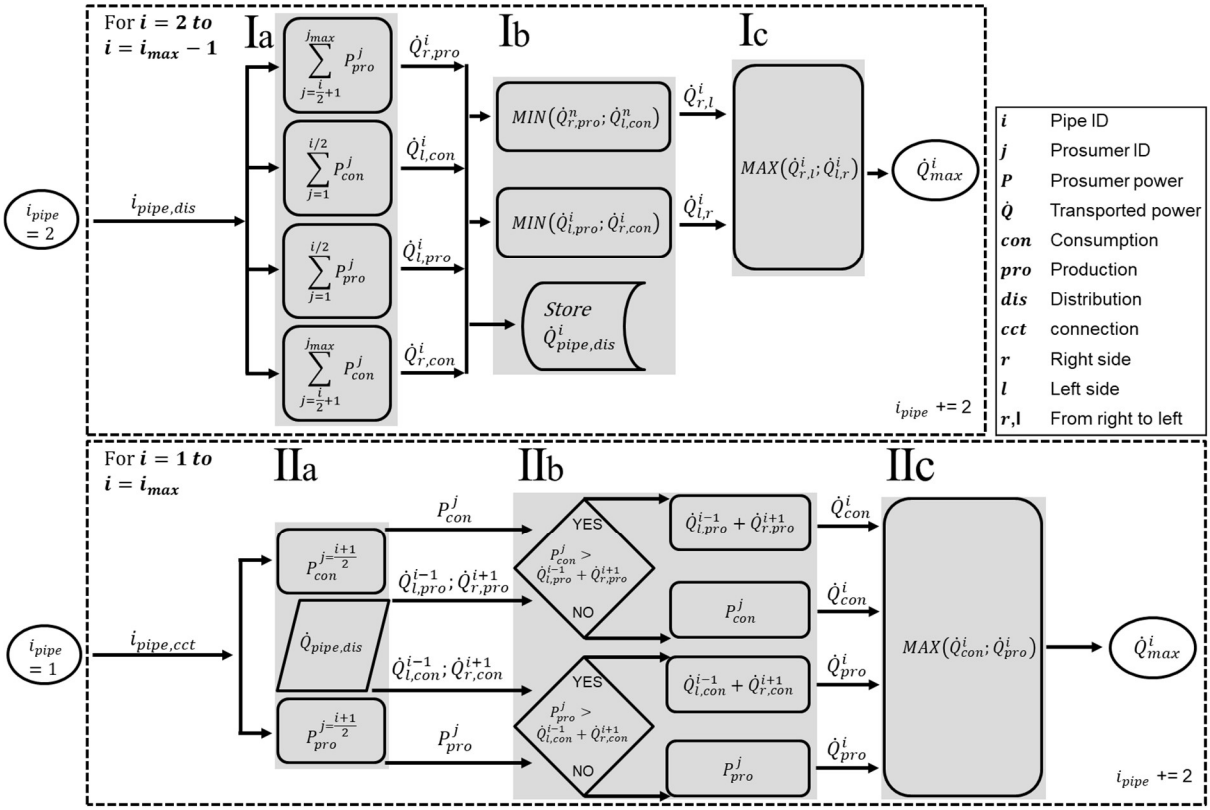

Figure 10: Detailed flow chart for the power determination algorithm: In Ia – Ic the maximum power exchange in distribution pipes is determined; in IIa - IIc the maximum transported power in the connection pipe is determined under consideration of the maximum power flows in the distribution pipes

Table 6 Pipe dimensions and designed power and volume flows

Pipe ID	DN	$D^{pipe}_{in,des}$ [mm]	u^{pipe}_{des} [m/s]	l_{route} [m]	R^{pipe}_{des} [Pa/m]	$\dot{Q}^i_{max}$ [kW]	$\dot{V}^i_{max}$ [m³/h]
1	25	27.3	0.70	10	215.51	25.27	1.47
2	25	27.3	0.70	40	215.51	25.27	1.47
3	25	27.3	0.59	10	160.58	21.51	1.25
4	32	36	0.74	40	171.35	46.78	2.72
5	25	27.3	0.59	10	157.03	21.24	1.24
6	40	41.9	0.74	49.5	140.80	63.07	3.67
7	32	36	0.66	10	139.58	41.83	2.44
8	25	27.3	0.59	46.5	157.03	21.24	1.24
9	25	27.3	0.59	10	157.03	21.24	1.24

Table 7 Control valve dimensions and designed operating points

Pros ID	Type	$\dot{V}^{CoV}_{des}$ [m³/h]	$\Delta p_{CoV,des}$ [kPa]	K^{CoV}_{vs} [m³/h]	a^{CoV}_{des} [-]
1	VUN015F320	1.47	83.36	1.6	0.42
2	VUN015F320	1.25	60.37	1.6	0.39
3	VUN015F320	1.24	58.91	1.6	0.41
4	VUN015F310	2.44	93.53	2.5	0.48
5	VUN015F320	1.24	58.91	1.6	0.34

Table 8 Pump dimensions and designed operating points

Pros. ID	Type	$\dot{V}^{FIP}_{des}$ [m³/h]	H^{FIP}_{des} [mH₂O]	H^{FIP}_{des} [kPa]
1	CR 1-7 A-A-A-E-HQQE	1.47	19.45	190.72
2	CR 1-7 A-A-A-E-HQQE	1.25	17.39	170.54
3	CR 1-7 A-A-A-E-HQQE	1.24	16.89	165.60
4	CR 3-5 A-A-A-E-HQQE	2.44	18.41	180.55
5	CR 1-7 A-A-A-E-HQQE	1.24	20.09	197.00

7 Literature

[1] isoplus Fernwärmetechnik Vertriebsgesellschaft mbH, *Planungshandbuch: Kapitel 1 - Allgemein.* [Online]. Verfügbar unter: https://www.isoplus.de/download/planungshandbuch.html (Zugriff am: 8. Juni 2022).

[2] J. Krimmling, *Energieeffiziente Nahwärmesysteme: Grundwissen, Auslegung, Technik für Energieberater und Planer*. Stuttgart: Fraunhofer-IRB-Verl., 2011.

[3] T. Nussbaumer, S. Thalmann, A. Jenni und J. Ködel, *Planungshandbuch Fernwärme,* 1. Aufl. Ittigen: EnergieSchweiz Bundesamt für Energie BFE, 2021.

[4] *Verenum.* [Online]. Verfügbar unter: http://www.verenum.ch/Dokumente_QMFW.html (Zugriff am: 10. Februar 2023).

[5] ASHRAE, *District Heating and Cooling Guides.* [Online]. Verfügbar unter: https://www.ashrae.org/technical-resources/bookstore/district-heating-and-cooling-guides (Zugriff am: 20. November 2022).

[6] Hochschule-Luzern, *Software Tools.* [Online]. Verfügbar unter: https://www.hslu.ch/de-ch/technik-architektur/ueber-uns/organisation/kompetenzzentren-und-forschungsgruppen/bau/gebaeudetechnik-und-energie/software-tools/ (Zugriff am: 10. Februar 2023).

[7] F. Bünning, M. Wetter, M. Fuchs und D. Müller, „Bidirectional low temperature district energy systems with agent-based control: Performance comparison and operation optimization“, *Applied Energy*, Jg. 209, S. 502–515, 2018, doi: 10.1016/j.apenergy.2017.10.072.

[8] L. Brange, J. Englund und P. Lauenburg, „Prosumers in district heating networks – A Swedish case study“, *Applied Energy*, Jg. 164, Nr. 1, S. 492–500, 2016, doi: 10.1016/j.apenergy.2015.12.020.

[9] T. Lickleder, T. Hamacher, M. Kramer und V. S. Perić, „Thermohydraulic model of Smart Thermal Grids with bidirectional power flow between prosumers“, *Energy*, Jg. 230, 2021, doi: 10.1016/j.energy.2021.120825.

[10] Hanne Kauko, Karoline Husevåg Kvalsvik, Daniel Rohde, Natasa Nord und Åmund Utne, „Dynamic modeling of local district heating grids with prosumers: A case study for Norway“, *Energy*, Jg. 151, S. 261–271, 2018, doi: 10.1016/j.energy.2018.03.033.

[11] G. Schweiger, P.-O. Larsson, F. Magnusson, P. Lauenburg und S. Velut, „District heating and cooling systems – Framework for Modelica-based simulation and dynamic optimization“, *Energy*, Jg. 137, Nr. 3, S. 566–578, 2017, doi: 10.1016/j.energy.2017.05.115.

[12] J. Lindhe, S. Javed, D. Johansson und H. Bagge, „A review of the current status and development of 5GDHC and characterization of a novel shared energy system“, *Science and Technology for the Built Environment*, Jg. 28, Nr. 5, S. 595–609, 2022, doi: 10.1080/23744731.2022.2057111.

[13] Marco Wirtz, Thomas Schreiber und Dirk Müller, „Survey of 53 5th Generation District Heating and Cooling (5GDHC) Networks in Germany“, 2022.

[14] Stephan-Arved Bröcker, „Ökologische und wirtschaftliche Bewertung von gebäudeübergreifenden Energiekonzepten für ein Quartier in München“. Masterthesis, Hochschule Augsburg, Augsburg, 2020.

[15] D. J. Zigrang und N. D. Sylvester, „Explicit approximations to the solution of Colebrook's friction factor equation“, *AIChE J.*, Jg. 28, Nr. 3, S. 514–515, 1982, doi: 10.1002/aic.690280323.

[16] *ISOPlus-Website.* [Online]. Verfügbar unter: https://www.isoplus.de/home.html (Zugriff am: 26. Januar 2023).

[17] Fr. Sauter AG, *2-Way Valve with Male Thread, PN16 - VUN On Fr. Sauter AG.* [Online]. Verfügbar unter: http://bim.sauter-controls.com/viewitems/regulating-valves/2-way-valve-with-male-thread--pn16---vun (Zugriff am: 26. Januar 2023).

[18] Grundfos Germany, *CR > Vertikale mehrstufige Kreiselpumpen / GG/1.4301.* [Online]. Verfügbar unter: https://product-selection.grundfos.com/de/products/cr?tab=products (Zugriff am: 26. Januar 2023).
[19] *Dymola – Dassault Systèmes®*. [Online]. Verfügbar unter: https://www.3ds.com/de/produkte-und-services/catia/produkte/dymola/ (Zugriff am: 24. Januar 2023).
[20] T. Lickleder, D. Zinsmeister und V. S. Perić, „A field-level control approach for bidirectional heat transfer stations in prosumerbased thermal networks: simulation and experimental evaluation: Presentation at “8th International Conference on Smart Energy Systems.“, S. 62–63. [Online]. Verfügbar unter: https://smartenergysystems.eu/wp-content/uploads/2022/09/BoA_SESAAU2022.pdf
[21] D. Zinsmeister *et al.,* „A Prosumer-Based Sector-Coupled District Heating and Cooling Laboratory Architecture“, *SSRN Journal*, 2022, doi: 10.2139/ssrn.4003819.
[22] *TABULA WebTool.* [Online]. Verfügbar unter: https://webtool.building-typology.eu/#bm (Zugriff am: 24. Januar 2023).
[23] M.-H. Kim, D.-W. Kim, D.-W. Lee und J. Heo, „Experimental Analysis of Bi-Directional Heat Trading Operation Integrated with Heat Prosumers in Thermal Networks“, *Energies*, Jg. 14, Nr. 18, S. 5881, 2021, doi: 10.3390/en14185881.
[24] T. Lickleder, D. Zinsmeister, I. Elizarov, V. Perić und P. Tzscheutschler, „Characteristics and Challenges in Prosumer-Dominated Thermal Networks“ (en), *J. Phys.: Conf. Ser.*, Jg. 2042, Nr. 1, 2021, doi: 10.1088/1742-6596/2042/1/012039.

Credit author statement

Fabian Speer: Writing - Original Draft, Methodology, Software, Investigation, Validation. Thomas Lickleder: Writing - Review & Editing, Supervision, Conceptualization, Methodology. Daniel Zinsmeister: Writing - Review & Editing, Conceptualization. Vedran Perić: Resources, Supervision, Writing - Review & Editing.